

Supporting Information for

Mesoscopic Structural Length Scales in P3HT/PCBM Mixtures Remain Invariant for Various Processing Conditions

Sameer Vajjala Kesava,¹ Rijul Dhanker,² Derek R. Kozub,¹ Kiarash Vakhshouri,¹ U Hyeok Choi,³ Ralph H. Colby,³ Cheng Wang,⁴ Alexander Hexemer,⁴ Noel C. Giebink² and Enrique D. Gomez^{1,5}*

¹Department of Chemical Engineering, The Pennsylvania State University, University Park, PA 16802

²Department of Electrical Engineering, The Pennsylvania State University, University Park, PA 16802

³Department of Materials Science and Engineering, The Pennsylvania State University, University Park, PA 16802

⁴Advanced Light Source, Lawrence Berkeley National Laboratory, Berkeley, CA 94720, USA

⁵Materials Research Institute, The Pennsylvania State University, University Park, PA 16802

1. Active layer thickness at various spin speeds for different casting solvents

Table S1 shows the spin speeds used to cast 1:1 by mass P3HT/PCBM films from various solvents and their respective thicknesses measured using a single-angle, single-wavelength ellipsometer. A profilometer was used for the film cast from chloroform at 1000 rpm due to significant surface roughness of the cast film.

Table S1. Thicknesses of films cast from different solvents at various spin speeds

Solvent	Spin speed (RPM)	Thickness (nm)
Chlorobenzene	1000	105 ± 4
	1500	88 ± 1
Chloroform	1000	181 ± 7
	7000	95 ± 2
Toluene	1000	149 ± 6
	3000	87 ± 2
<i>o</i> -xylene	1000	111 ± 8
	1650	83 ± 5

2. Charge mobilities extracted from thin film transistor measurements

In order to characterize the charge mobility of P3HT used in our study we fabricated and tested thin-film transistors as described previously.¹ Briefly, bottom-contact, bottom-gate field-effect transistors were made using heavily doped p-type Si wafers as the gate electrodes with a 300 nm-thick thermally grown SiO₂ layer as the gate dielectric ($C = 10.6 \text{ nF/Cm}^2$, Process Specialties). Wafers were cleaned through sonication for 20 min in acetone followed by sonication in isopropanol for 20 min. Gold source and drain electrodes (with a thickness of $\approx 100 \text{ nm}$) were deposited through conventional double-layer lithography with channel widths of 220 μm and lengths of 20 μm . After 10 min of UV-ozone cleaning, substrates were placed in a jar of 16 mL hexadecane and 20 μL of trimethoxy(octadecyl)silane was added. After 12 h, trimethoxy(octadecyl)silane treated substrates were cleaned by rinsing with isopropanol. Solutions of P3HT were made with anhydrous chlorobenzene (Sigma–Aldrich) in a N₂ glovebox.

Solutions were stirred for a minimum of 12 h at room temperature and heated to 75 °C for 30 s prior to use to ensure dissolution. Films were cast from 10 mg mL⁻¹ solutions at 1000 rpm for 1 min yielding film thicknesses of ca. 40 nm. Ten devices were tested. The transistor characteristics are shown in Figure S1 for a representative device. The average charge mobility of ten devices is 0.05 ± 0.01 cm²/Vs, where the error is the standard deviation.

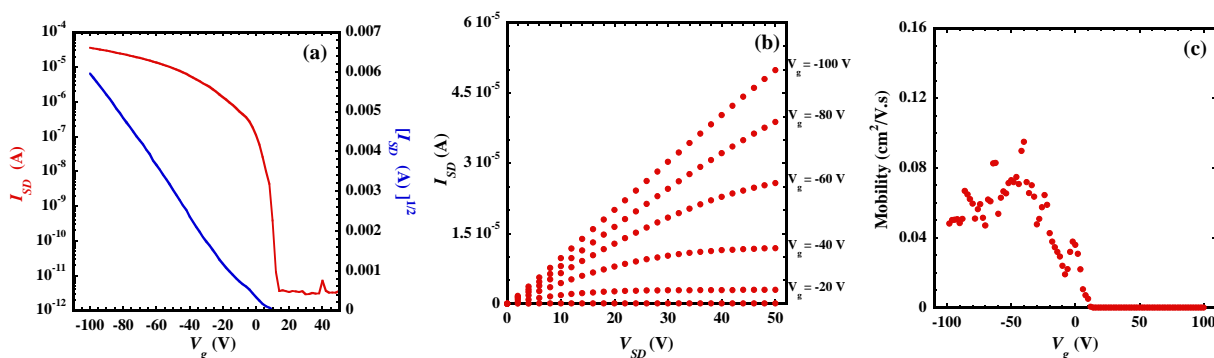


Figure S1. Transfer characteristics of a representative P3HT transistor. (a) Source-drain current (I_{SD}) vs gate voltage (V_g) with a source-drain voltage (V_{SD}) of 50 V, (b) source-drain current vs source-drain voltage for various gate voltages and (c) mobility as a function of gate voltage. We take the mobility of this device to be 0.06 cm²/Vs.

3. Rheometry of P3HT

Rheological measurements were performed using a Rheometrics RDS-II with a parallel plate geometry. Approximately 1 mm thick samples were placed in 8 mm diameter plates and pressed at 240 °C. Experiments were performed in an N₂ atmosphere. Figure S2 shows the shear storage (G') and loss modulus (G'') as a function of frequency for P3HT taken at 230 °C. The frequency-independent G' is a clear signature of solid-like behavior due to tie chains connecting the crystallites within P3HT.

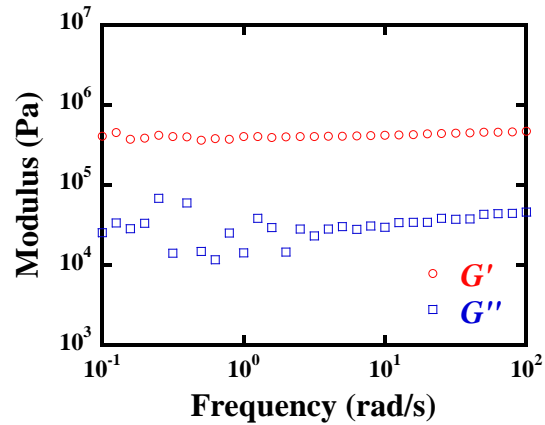


Figure S2. Storage (G') and loss (G'') modulus as a function of frequency for neat P3HT at 230 °C. The frequency-independent G' clearly indicates solid-like behavior and the presence of tie chains connecting crystallites.

4. Comparison of GISAXS data to FFTs of sulfur maps

Figure S3a shows the in-plane GISAXS intensity for an annealed P3HT/PCBM sample and the corresponding Teubner-Strey (TS) fit from which the domain spacing is obtained. The fitting is described in detail in reference ². Figure S3b shows the corresponding Teubner-Strey fits for azimuthally-averaged Fast Fourier Transform intensities obtained from elemental maps of Figure 2 of the main text.

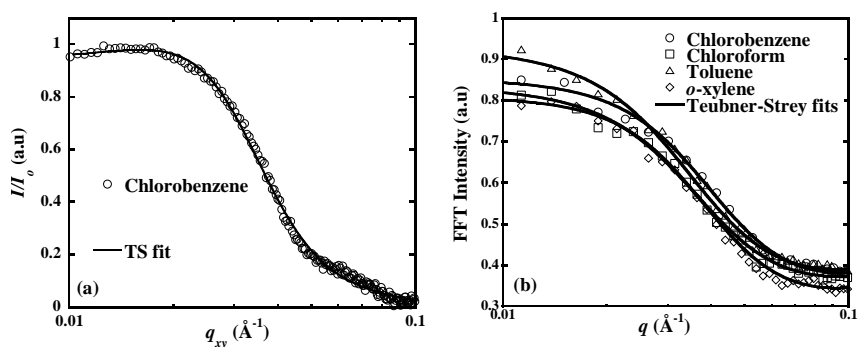


Figure S3. (a) GISAXS intensity vs in-plane scattering vector, q_{xy} , for a P3HT/PCBM film cast from chlorobenzene with the corresponding Teubner-Strey (TS) fit. Only one TS fit is shown for clarity. (b) Intensity vs scattering vector, q , obtained from azimuthally integrated Fast Fourier Transforms of the sulfur maps shown in Figure 2 of the main text and their respective TS fits.

5. Domain spacing at different annealing temperatures

Figure S4 compares the domain spacing in the active layer of P3HT/PCBM films spun-cast from four solvents and annealed at 150°C and 180°C. Domain spacings were obtained from fitting the Teubner-Strey equation to GISAXS intensities.

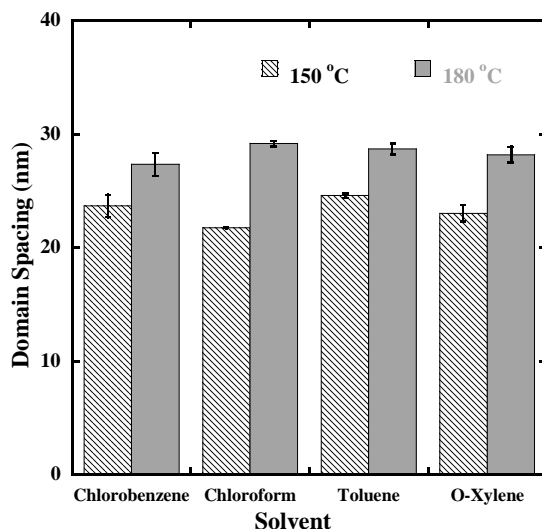


Figure S4. Domain spacing for 1:1 by mass P3HT/PCBM films and annealed at 150°C and 180°C for 15 min. Error bars represent the standard deviation from multiple measurements.

6. Composition of P3HT in the PCBM-rich phase

Table S2 shows the composition of P3HT in the PCBM-rich phase of the elemental maps shown in Figure 2 of the main text determined from images as described previously.²⁻⁴

Casting solvent	Volume fraction P3HT in PCBM-rich phase
Chlorobenzene	0.29 ± 0.05
Chloroform	0.28 ± 0.02
Toluene	0.28 ± 0.01
<i>o</i> -xylene	0.30 ± 0.05

7. Comparison of device characteristics

Tables S3 contains the performance characteristics of 1:1 by mass P3HT/PCBM solar cells: efficiency (η), short-circuit current density (J_{SC}), open circuit voltage (V_{OC}), fill factor (FF), series resistance (R_S), shunt resistance (R_{SH}), ideality factor (m) and dark saturation current density (J_0). R_S , R_{SH} , m and J_0 were obtained by fitting the diode equation⁵ to the measured J - V curves in Figure 4 of the main text. Data in Table S3 is from devices where the active layer was cast from various spin-casting solvents at 1000 rpm and consequently the active layer thicknesses differ. Table S4 shows the characteristics of solar cells where the active layer was cast using various spin speeds as tabulated in Table S1. As such, the characteristics in Table S4 are for devices whose active layer thicknesses are roughly invariant.

Table S3. Device characteristics and diode parameters of 1:1 by mass P3HT/PCBM devices, spun-cast at 1000 rpm and annealed at 150°C for 15 min

	η (%)	J_{SC} (mA/cm ²)	V_{OC} (V)	FF	R_S (Ω -cm ²)	$R_{SH} \times 10^{-3}$ (Ω -cm ²)	m	J_o (μ A/cm ²)
Chlorobenzene	2.1 ± 0.2	6.7 ± 0.5	0.52 ±	0.56 ±	7.46 ±	1.14 ±	2.92 ±	10.3 ±
			0.02	0.03	3.21	0.21	0.37	11.8
Chloroform	2.6 ± 0.2	8.3 ± 0.7	0.54 ±	0.55 ±	7.05 ±	1.39 ±	2.95 ±	14.4 ±
			0.02	0.03	3.34	0.28	0.54	11.0
Toluene	1.9 ± 0.1	6.2 ± 0.2	0.50 ±	0.54 ±	1.22 × 10	1.35 ±	2.61 ±	3.97 ±
			0.01	0.03	± 1.65	0.48	0.14	2.01
<i>o</i> -xylene	2.0 ± 0.1	7.0 ± 0.3	0.50 ±	0.56 ±	7.14 ±	1.00 ±	2.81 ±	6.27 ±
			0.03	0.02	2.09	0.18	0.32	3.32

Table S4. Device characteristics and diode parameters of 1:1 by mass P3HT/PCBM devices, spun-cast at variable rpm and annealed at 150°C for 15 min

	<i>Efficiency</i> (%)	J_{SC} (mA/cm ²)	V_{OC} (V)	FF	R_S (Ω -cm ²)	$R_{SH} \times 10^{-3}$ (Ω -cm ²)	m	J_o (μ A/cm ²)
Chlorobenzene (1500 rpm)	2.0 ± 0.1	6.7 ± 0.2	0.49 ±	0.55 ±	7.91 ±	1.00 ±	2.76 ±	9.36 ± 9.89
			0.01	0.02	2.95	0.18	0.24	
Chloroform (7000 rpm)	2.1 ± 0.1	6.6 ± 0.1	0.49 ±	0.57 ±	7.57 ±	1.00 ±	2.62 ±	6.13 ± 6.79
			0.02	0.02	2.12	0.23	0.26	
Toluene (3000 rpm)	2.0 ± 0.1	6.7 ± 0.3	0.49 ±	0.55 ±	8.43 ±	1.00 ±	2.79 ±	8.36 ± 4.83
			0.03	0.02	2.17	0.36	0.30	
<i>o</i> -xylene (1650 rpm)	2.0 ± 0.2	6.8 ± 0.2	0.47 ±	0.56 ±	5.33 ±	1.18 ±	2.87 ±	1.58 × 10 ±
			0.04	0.02	2.08	0.56	0.36	1.02 × 10

8. Estimation of number of photons absorbed in the active layer using optical modeling

Figure S5 shows the real (n) and imaginary (k) parts of the complex refractive index as a function of wavelength for different layers in solar cells (glass, ITO, PEDOT:PSS, 1:1 P3HT/PCBM annealed film spun-cast from chlorobenzene, and aluminum). Because the transmittance of glass is greater than 90% at all wavelengths in the relevant range, k for glass is taken to be zero. This data was obtained from analysis of spectroscopic ellipsometer measurements and was used in the simulation of number of photons absorbed in the active layer (Figure S6).

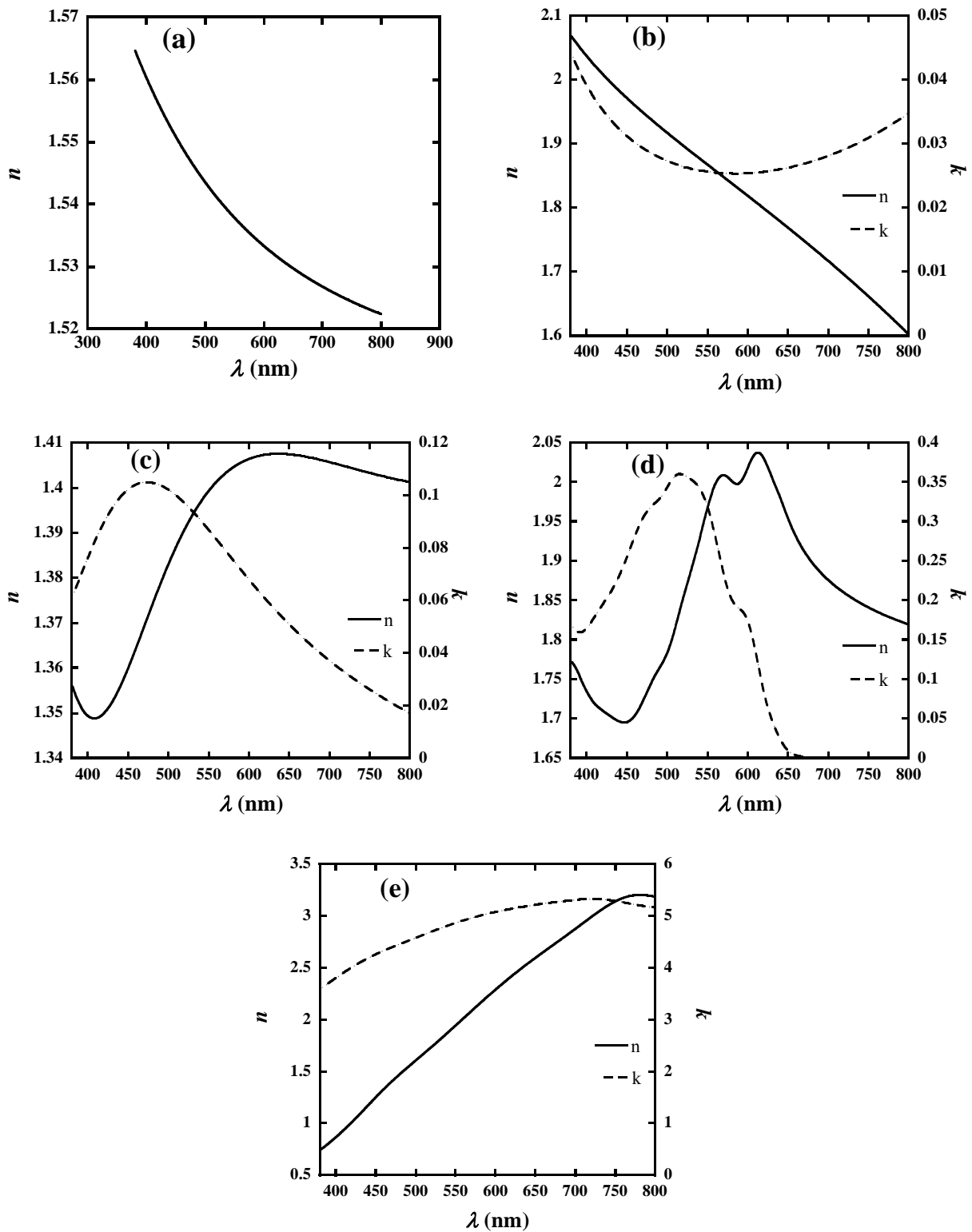


Figure S5. Complex refractive indices, n and k , of (a) glass, (b) ITO, (c) PEDOT:PSS, (d) 1:1 by mass P3HT/PCBM mixture annealed at 150°C for 15 min and (e) aluminum, as a function of wavelength. Data was obtained from variable-angle spectroscopic ellipsometry.

Figure S6 shows the number of photons absorbed in the active layer of P3HT/PCBM solar cells as a function of thickness. This was calculated from the Transfer Matrix Formalism (TMF) method, implemented by Pettersson et al., and explained in detail in references 6-8. This method allows for calculation of the distribution of electric field within the device taking interference effects into account, and requires a complex refractive index $n + i k$ of all the layers of the device (Glass (1 mm)/ ITO (84 nm)/ PEDOT:PSS (50 nm)/ P3HT:PCBM (x nm)/ Aluminum (75 nm)). The refractive indices were obtained using spectroscopic ellipsometry (Figure S5). The number of photons absorbed upon normal incidence is proportional to the product of n , k and squared modulus of the electric field at that particular position in the device.

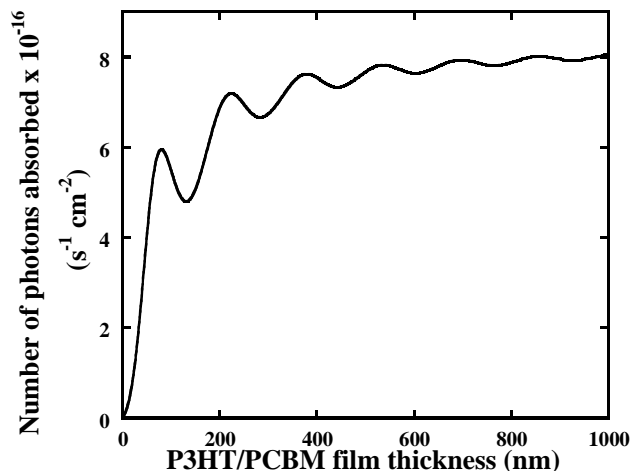


Figure S6. Number of photons absorbed in the active layer of 1:1 by mass P3HT/PCBM devices as a function of the thickness of the active layer.

9. UV-visible absorbance of P3HT/PCBM active layers

Figure S7 shows the UV-visible absorbance of 1:1 P3HT/PCBM annealed films spun-cast from the four solvents. The spin-casting speed was allowed to vary in order to achieve similar thicknesses (~ 90 nm, Table S1) as measured through spectroscopic ellipsometry. The similar absorption spectra confirm that all films have a similar thickness.

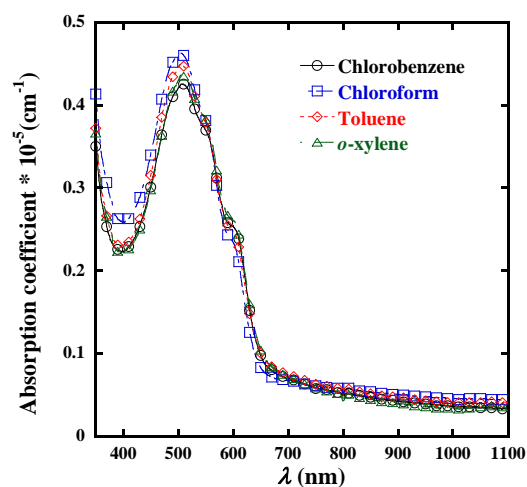


Figure S7. UV-Visible absorbance for 1:1 by mass P3HT/PCBM films spun-cast from different solvents having similar thicknesses (ca. 90 nm). Films were annealed at 150°C for 15 min.

10. Comparison of device characteristics of devices annealed after cathode deposition

Figure S8 shows the average J - V curves of 1:1 by mass P3HT/PCBM solar cells spun-cast using various spin speeds (Table S1) and annealed at 150 °C for 15 min after cathode deposition. The efficiency (η), short-circuit current density (J_{SC}), open circuit voltage (V_{OC}), fill factor (FF), series resistance (R_s), shunt resistance (R_{SH}), ideality factor (m) and dark saturation current density (J_0) obtained from the device data shown in Figure S8 are tabulated in Table S5. R_s , R_{SH} , m and J_0 were obtained by fitting the diode equation⁵ to the measured J - V curves shown in Figure S8.

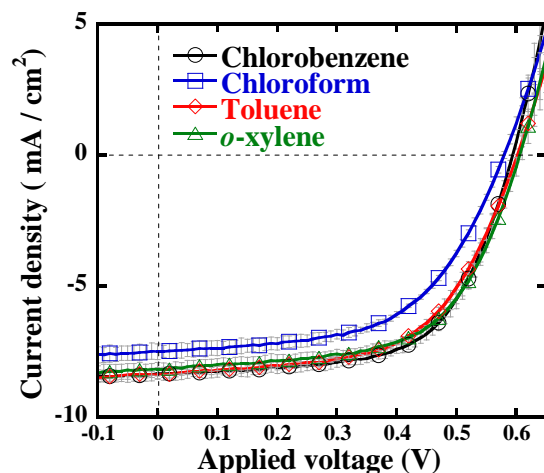


Figure S8. Average current densities vs applied bias for 1:1 by mass P3HT/PCBM solar cells where the photoactive layer was spun cast at various rpm such that the thickness is roughly the same (~ 90 nm). All devices were annealed at 150°C for 15 min after Al deposition. The error bars represent the standard deviation from multiple measurements.

Table S5. Device characteristics and diode parameters of 1:1 by mass P3HT/PCBM devices, spun-cast at variable rpm and post-annealed at 150°C for 15 min

	<i>Efficiency</i> (%)	J_{SC} (mA/cm ²)	V_{OC} (V)	<i>FF</i>	R_S (Ω -cm ²)	$R_{SH} \times 10^{-3}$ (Ω -cm ²)	<i>m</i>	J_o (μ A/cm ²)
Chlorobenzene (1500 rpm)	3.14 ± 0.1	8.4 ± 0.2	0.59 ± 0.01	0.62 ± 0.02	6.06 ± 2.46	1.08 ± 0.13	1.97 ± 0.12	$7.77 \times 10^{-2} \pm 4.75 \times 10^{-2}$
Chloroform (7000 rpm)	2.57 ± 0.1	7.5 ± 0.3	0.58 ± 0.01	0.56 ± 0.02	7.86 ± 2.70	1.18 ± 0.34	2.72 ± 0.34	2.57 ± 2.47
Toluene (3000 rpm)	3.04 ± 0.1	8.4 ± 0.2	0.60 ± 0.01	0.58 ± 0.02	7.86 ± 2.46	1.08 ± 0.16	2.48 ± 0.22	$8.25 \times 10^{-1} \pm 5.91 \times 10^{-1}$
<i>o</i> -xylene (1650 rpm)	3.07 ± 0.1	8.1 ± 0.3	0.61 ± 0.01	0.60 ± 0.02	6.44 ± 2.58	1.00 ± 0.17	2.23 ± 0.16	$2.51 \times 10^{-1} \pm 1.82 \times 10^{-1}$

11. Internal quantum efficiency of devices annealed after cathode deposition

Figure S9 shows the internal quantum efficiencies (IQE) of devices fabricated from four different solvents (Figure S8) and annealed at 150 °C for 15min after cathode deposition. The

total number of photons absorbed by the active layer was obtained from optical modeling (Figure S6) and was utilized in the calculation of IQE. The figure shows that, similar to devices annealed prior to cathode deposition, the IQE of post-annealed devices is invariant between the different casting solvents.

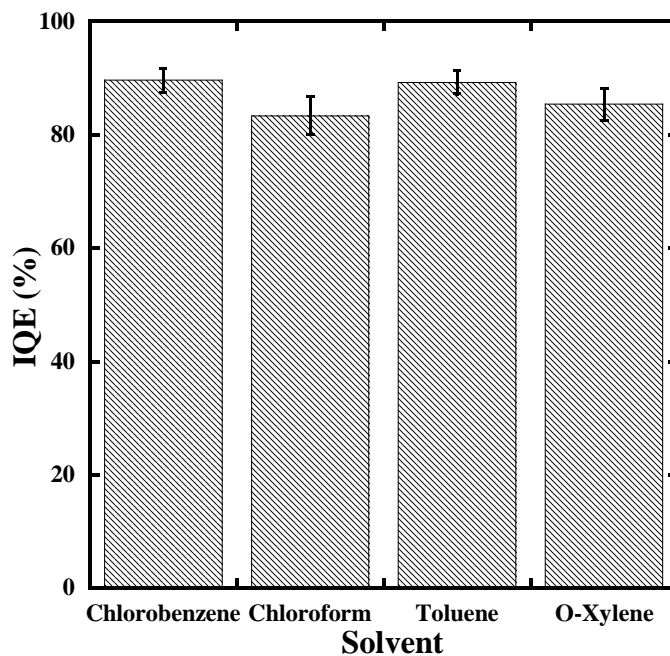


Figure S9. Overall internal quantum efficiencies for 1:1 by mass P3HT/PCBM solar cells cast from various solvents and annealed at 150°C for 15 min post aluminum deposition. The number of photons absorbed was obtained from optical modeling results shown in Figure S6.

12. Device characteristics for various processing conditions

Tables S6 to S9 contain the device characteristics for P3HT/PCBM devices shown in Figure 6 of the main text. Films were cast from chlorobenzene.

Table S6. Efficiency (%)

Annealing time (min)	10	30	60
Annealing temperature (°C)			
100	1.3 ± 0.1	1.4 ± 0.1	1.4 ± 0.1
140	1.9 ± 0.1	2.0 ± 0.1	1.9 ± 0.1
165	2.0 ± 0.1	2.0 ± 0.1	1.9 ± 0.1
190	1.7 ± 0.1	1.6 ± 0.1	1.6 ± 0.1

Table S7. Short-circuit current density (J_{SC}) (mA/cm²)

Annealing time (min)	10	30	60
Annealing temperature (°C)			
100	5.3 ± 0.2	5.4 ± 0.2	5.7 ± 0.2
140	6.8 ± 0.1	6.8 ± 0.2	7.0 ± 0.1
165	7.0 ± 0.1	7.0 ± 0.2	6.7 ± 0.5
190	6.7 ± 0.5	6.2 ± 0.4	6.4 ± 0.2

Table S8. Open-circuit voltage (V_{oc}) (V)

Annealing time (min)	10	30	60
Annealing temperature (°C)			
100	0.48 ± 0.01	0.48 ± 0.01	0.48 ± 0.02
140	0.57 ± 0.01	0.57 ± 0.06	0.57 ± 0.01
165	0.50 ± 0.01	0.54 ± 0.01	0.49 ± 0.01
190	0.47 ± 0.06	0.46 ± 0.06	0.49 ± 0.03

Table S9. Fill factor

Annealing time (min)	10	30	60
Annealing temperature (°C)			
100	0.51 ± 0.01	0.52 ± 0.02	0.50 ± 0.01
140	0.48 ± 0.01	0.52 ± 0.02	0.47 ± 0.01
165	0.56 ± 0.03	0.54 ± 0.02	0.57 ± 0.03
190	0.53 ± 0.02	0.54 ± 0.02	0.52 ± 0.02

13. References

1. Vakhshouri, K.; Gomez, E. D., Effect of Crystallization Kinetics on Microstructure and Charge Transport of Polythiophenes. *Macromolecular Rapid Communications* **2012**, 33, (24), 2133-2137.
2. Kozub, D. R.; Vakhshouri, K.; Orme, L. M.; Wang, C.; Hexemer, A.; Gomez, E. D., Polymer Crystallization of Partially Miscible Polythiophene/Fullerene Mixtures Controls Morphology. *Macromolecules* **2011**, 44, (14), 5722-5726.
3. Egerton, R. F., *Electron energy-loss spectroscopy in the electron microscope*. 2nd ed.; Plenum Press: New York, 1996; p xi, 485 p.
4. Guo, C.; Kozub, D. R.; Vajjala Kesava, S.; Wang, C.; Hexemer, A.; Gomez, E. D., Signatures of Multiphase Formation in the Active Layer of Organic Solar Cells from Resonant Soft X-ray Scattering. *ACS Macro Letters* **2013**, 2, 185-189.
5. Nelson, J., *The physics of solar cells*. Imperial College Press: London, 2003; p xix, 363 p.
6. Knittl, Z., *Optics of thin films : an optical multilayer theory*. Wiley: London ; New York, 1976; p 548 p.
7. Macleod, H. A., *Thin-film optical filters*. 4th ed.; CRC Press/Taylor & Francis: Boca Raton, FL, 2010; p xviii, 782 p.
8. Pettersson, L. A. A.; Roman, L. S.; Inganas, O., Modeling photocurrent action spectra of photovoltaic devices based on organic thin films. *Journal of Applied Physics* **1999**, 86, (1), 487-496.